Bismuth-stabilized $c(2\times6)$ reconstruction on a InSb(100) substrate: Violation of the electron counting model

P. Laukkanen,[1,2,*] M. P. J. Punkkinen,[1,3,†] N. Räsänen,[1] M. Ahola-Tuomi,[1] M. Kuzmin,[1,4] J. Lång,[1] J. Sadowski,[5,6] J. Adell,[7,6] R. E. Perälä,[1] M. Ropo,[8] K. Kokko,[1] L. Vitos,[3,9,10] B. Johansson,[3,9,11] M. Pessa,[2] and I. J. Väyrynen[1]

[1]*Department of Physics and Astronomy, University of Turku, FI-20014 Turku, Finland*

[2]*Optoelectronics Research Centre, Tampere University of Technology, FI-33101 Tampere, Finland*

[3]*Applied Materials Physics, Department of Materials Science and Engineering, Royal Institute of Technology, SE-10044 Stockholm, Sweden*

[4]*A. F. Ioffe Physico-Technical Institute, Russian Academy of Sciences, St. Petersburg 194021, Russian Federation*

[5]*Institute of Physics, Polish Academy of Sciences, al. Lotnikow 32/46, 02-668 Warszawa, Poland*

[6]*MAX-lab, Lund University, SE-221 00 Lund, Sweden*

[7]*Department of Applied Physics, Chalmers University of Technology, SE-41296 Göteborg, Sweden*

[8]*Department of Information Technology, Åbo Akademi University, FI-20500 Turku, Finland*

[9]*Division for Materials Theory, Department of Physics and Materials Science, Uppsala University, SE-75121 Uppsala, Sweden*

[10]*Research Institute for Solid State Physics and Optics, P.O. Box 49, H-1525 Budapest, Hungary*

[11]*School of Physics and Optoelectronic Technology, College of Advanced Science and Technology, Dalian University of Technology, Dalian 116024, China*

(Received 15 April 2009; revised manuscript received 18 November 2009; published 8 January 2010)

By means of scanning tunneling microscopy/spectroscopy (STM/STS), photoelectron spectroscopy, and first-principles calculations, we have studied the bismuth (Bi) adsorbate-stabilized InSb(100) substrate surface which shows a $c(2\times6)$ low-energy electron diffraction pattern [thus labeled Bi/InSb(100)$c(2\times6)$ surface] and which includes areas with metallic STS curves as well as areas with semiconducting STS curves. The first-principles phase diagram of the Bi/InSb(100) surface demonstrates the presence of the Bi-stabilized metallic $c(2\times6)$ reconstruction and semiconducting (4×3) reconstruction depending on the chemical potentials, in good agreement with STS results. The existence of the metallic $c(2\times6)$ phase, which does not obey the electron counting model, is attributed to the partial prohibition of the relaxation in the direction perpendicular to dimer rows in the competing reconstructions and the peculiar stability of the Bi-stabilized dimer rows. Based on (i) first-principles phase diagram, (ii) STS results, and (iii) comparison of the measured and calculated STM and photoemission data, we show that the measured Bi/InSb(100)$c(2\times6)$ surface includes metallic areas with the stable $c(2\times6)$ atomic structure and semiconducting areas with the stable (4×3) atomic structure.

DOI: 10.1103/PhysRevB.81.035310 PACS number(s): 68.35.−p, 81.10.−h, 73.20.−r, 68.47.Fg

I. INTRODUCTION

The $c(2\times6)$ reconstruction commonly appears on the III-Sb(100) substrate surfaces in the Sb-rich experimental conditions. The knowledge of the properties of this particular surface structure is important to understand and control [e.g., with reflection high-energy electron diffraction (RHEED)] the epitaxial growth of III-Sb materials for electronics devices since the growth usually proceeds via the $c(2\times6)$-reconstructed substrate.

Previous photoemission studies combined with scanning tunneling microscopy (STM) and RHEED observations have revealed that the chemical compositions of the Sb/III-Sb(100)(1×3) and $-c(2\times6)$ surfaces differ from each other, and two distinct atomic models, shown in Figs. 1(a) and 1(b), have been proposed for them, respectively.[1,2] However, there are indications that the detailed structures of the (1×3) and $c(2\times6)$ surfaces have remained unresolved.[3–6] Indeed, structures, shown in Figs. 2(a)–2(e), have been recently proposed for them on the basis of high-resolution STM findings and theoretical calculations.[7] Separate total-energy calculations supported these models,[8] which show that the Sb/III-Sb(100) surfaces are, in fact, composed of (4×3) unit cells including mixed III-Sb dimers. Another significant difference is that the models in Figs. 2(a)–2(e) obey the electron counting model (ECM),[9–11] but those in Figs. 1(a) and 1(b) do not. In passing, the $c(4\times4)$ model in Fig. 1(c) obeys ECM but that in Fig. 2(f) does not. Therefore, the surfaces described with the models in Figs. 1(a) and 1(b) should be metallic, while the models in Figs. 2(a)–2(e) lead to the semiconducting Sb/III-Sb(100) reconstructions according to the ECM.[12] Thus, the recent findings of the (4×3) building blocks support the view according to which the tendency for the semiconducting surface structure through the ECM is an important driving force behind the Sb/III-Sb(100) reconstructions. A III-V surface satisfies the ECM if all dangling bonds of the more electropositive element (in this case In) are empty and all dangling bonds of the more electronegative element (Sb) are full, which leads to semiconducting state.[11] In addition to the ECM, two other physical factors, which commonly affect the reconstruction formation, are tendencies to decrease the amount of the dangling bonds as well as the electrostatic energy due to the arrangement of the occupied dangling bonds.

In this paper, low-energy electron diffraction (LEED), STM/scanning tunneling spectroscopy (STM/STS), and photoemission measurements reveal first that the group-V ele-

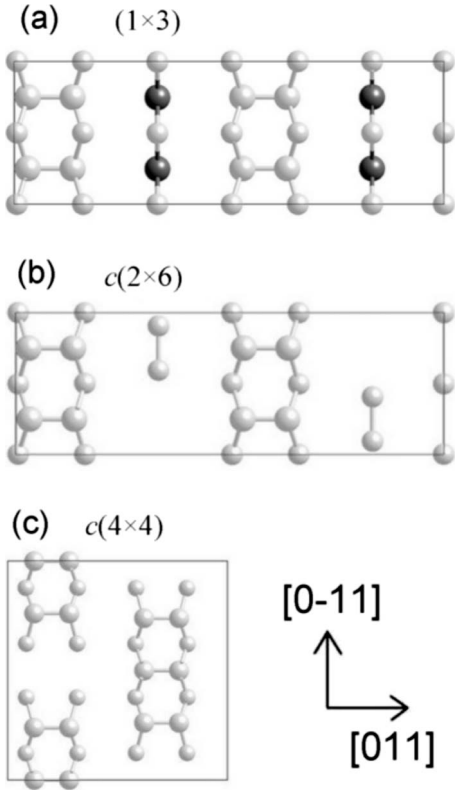

FIG. 1. Atomic models for some group-V-rich reconstructions on the III-Sb(100) surfaces, labeled as follows: (a) (1×3), (b) $c(2\times6)$, and (c) $c(4\times4)$. The group-III atoms are shown by black spheres and the group-V atoms by gray spheres. The first layer atoms are shown by larger spheres than the second-layer atoms. Atoms in deeper layers are not shown.

ment bismuth (Bi) induces on the InSb(100) substrate the surface reconstruction which produces a clear $c(2\times6)$ LEED pattern and includes ordered areas with metallic STS current-voltage (*I-V*) curves as well as the areas with semiconducting *I-V* curves. [This measured surface is labeled Bi/InSb(100)$c(2\times6)$ hereafter.] Then careful *ab initio* total-energy calculations demonstrate the presence of the Bi-stabilized metallic $c(2\times6)$ reconstruction and semiconducting (4×3) reconstruction depending on the chemical potentials and further elucidate the physical mechanisms that stabilize the $c(2\times6)$ phase, which does not obey the ECM. The total-energy calculations elucidate also the phase diagram of the pure Sb-stabilized InSb(100) surface. Moreover, by combining (i) first-principles phase diagram, (ii) STS results, and (iii) comparison of the measured and calculated STM and photoemission data, we show that the measured Bi/InSb(100)$c(2\times6)$ surface includes metallic areas with the stable $c(2\times6)$ atomic structure and also semiconducting areas with the stable (4×3) atomic structure. The knowledge of the Bi/InSb(100)$c(2\times6)$ surface properties is essential not only for understanding the detailed formation mechanisms of the technologically important $c(2\times6)$ reconstructions but also for understanding the Bi surfactant-mediated growth of III-V's.[13,14] The Bi/InSb(100)$c(2\times6)$ substrate also represents a starting surface to study the growth

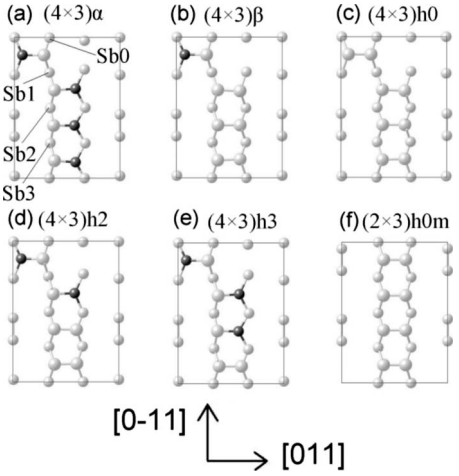

FIG. 2. Atomic models for some group-V-rich reconstructions on the III-Sb(100) surfaces, labeled as follows: (a) $(4\times3)\alpha$, (b) $(4\times3)\beta$, (c) (4×3)h0, (d) (4×3)h2, (e) (4×3)h3, and (f) (2×3)h0m. The group-III atoms are shown by black spheres and the group-V atoms by gray spheres. The first-layer atoms are shown by larger spheres than the second-layer atoms. Atoms in deeper layers are not shown.

phenomena of the epitaxial Bi and MnBi films,[15–17] which both are almost lattice matched to the InSb substrates.

Previously, the ECM breakage has been found at least on the following surfaces: GaSb(100)$(n\times5)$,[18] Sb/GaAs(111)(1×3),[19] and Bi/III-V(100)(2×1).[20–22] It has been shown that the replacement of some Sb atoms by Ga ones in GaSb(100)$(n\times5)$ reconstructions decreases the metallicity and surface energy.[23] Furthermore, the stabilization of Bi/III-V(100)(2×1) has been found to arise from the increased interaction in the dimer rows, which was demonstrated by the energy bands and the electron charge-density contours, and from the surface-stress relief.[22] These effects were connected to the geometrical structure of the Bi-stabilized surfaces.[22]

In this point, we would like still to remind the reader of the fact that the considered reconstruction periodicities are sometimes used ambiguously. For example, dependent on the measurement by which the periodicity has been determined (e.g., RHEED vs STM), the same surface might have been called (1×3) or $c(2\times6)$. Later, the measurements and calculations have revealed, as described above, that the real reconstruction is (4×3) and not (1×3). Still, sometimes it is talked about the (1×3) reconstruction. The apparent features of the (1×3), $c(2\times6)$, and (4×3) reconstructions are similar since all of them consist of the dimer rows with the $\times3$ separation. Moreover, it has been recently shown that the (1×3) and $c(2\times6)$ diffraction patterns from GaSb are due to different types of disorder of the (4×3) units.[24]

II. EXPERIMENTS

Measurements were done in two separate ultrahigh-vacuum (UHV) systems both equipped with LEED and sputtering instruments. STM images were taken in the constant current mode and the current-voltage curves were obtained

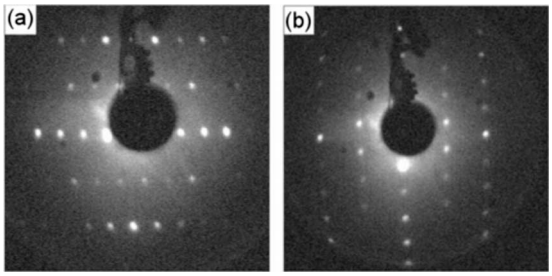

FIG. 3. (a) LEED pattern (44 eV) from the starting InSb(100)$c(8\times2)$ substrate. (b) LEED pattern (39 eV) from the Bi/InSb(100)$c(2\times6)$ surface.

by STS mode simultaneously with the topographic measurement of ordered surface areas. Photoemission was done at the MAX laboratory in Sweden (the Beamline 41) using an angle-resolving analyzer with an acceptance angle of about 2°. The incident-beam angle was 45° relative to the surface. All measurements were done at room temperature (RT).

InSb(100) substrates were cleaned by the cycles of argon-ion sputtering (1 keV, 10 mA) for 0.5 h at the substrate temperature of about 300 °C and subsequent heating of the substrate to about 440 °C in UHV for 0.5 h. Six cycles were required until a clear $c(8\times2)$ LEED pattern in Fig. 3(a) was obtained and until the In oxide related emission disappeared in the In 4*d* core-level spectra. It was also concluded that a density of possible sputtering-induced In droplets on our substrates was not significant, concerning the results shown below, since no emission shoulder from metallic In droplets[25] was seen in our In 4*d* spectra. Approximately 1.5-monolayer-thick Bi layer was deposited on the clean InSb(100)$c(8\times2)$ surface held at RT. Heating this Bi/InSb sample at 200–250 °C for 2 h produced a clear $c(2\times6)$ LEED pattern shown in Fig. 3(b). When the sample was heated above 250 °C, LEED changed to a combined pattern of $c(2\times6)$ and $c(8\times2)$. Around 300 °C, the $2\times$ spots were so weak that we could not resolve whether it was a (1×3) or $c(2\times6)$ pattern combined with the $c(8\times2)$. Temperatures were measured by a pyrometer.

III. CALCULATIONS

Theoretical calculations were performed using the *ab initio* density-functional total-energy code with the local-density approximation (LDA).[26,27] The approach is based on plane-wave basis and projector augmented wave method[28,29] [Vienna *ab initio* simulation package, (VASP)].[30–33] The reconstructions in Figs. 1 and 2 were simulated by (4×3) and (2×6) slabs, including 16 atomic layers and treating the *d* electrons as core electrons. The dangling bonds of the bottom surface In atoms were passivated by pseudohydrogen atoms ($Z=1.25$). Theoretical LDA lattice constants (4.29 Å for GaSb and 4.58 Å for InSb) were used in most of the calculations, and two bottom atomic layers of the slabs were fixed to the ideal bulk positions. Other atoms, including the pseudohydrogen atoms, were relaxed until the remaining forces were less than 20 meV/Å. The energy cutoff was 250 eV. The number of *k* points in the surface Brillouin zone was 12 [9 and 16 for $c(4\times4)$]. The *k*-point sampling was performed by the Monkhorst-Pack scheme[34] with the origin shifted to the Γ point. Our tests showed that these parameters lead to accurate surface energies. The estimated errors in the relative surface energies are of the order of meV/(1×1) area. Surface core-level shifts (SCLSs) were calculated within the initial state model.[35,36] The formed surface structure depends on the deposition conditions. The relative stabilities of the considered reconstructions can be determined by the surface free energy and the chemical potentials (μ_i) of the surface constituents (i=Bi,In,Sb).[37,38] The surface energy γ is calculated by

$$\gamma A = E_{\text{tot}} - n_{\text{Sb}}\mu_{\text{InSb}} - (n_{\text{In}} - n_{\text{Sb}})\mu_{\text{In}} - n_{\text{Bi}}\mu_{\text{Bi}}, \qquad (1)$$

where n_i denotes the number of atoms of type i in the unit cell, the μ_{InSb} is the chemical potential for the InSb compound, and the E_{tot} is the total energy of the unit cell. The chemical potentials depend on the deposition conditions, and the μ_{In} and μ_{Sb} are connected to each other by

$$\mu_{\text{In}} + \mu_{\text{Sb}} = \mu(\text{InSb})_{\text{bulk}}. \qquad (2)$$

The chemical potentials for the bulk structures were calculated by using orthorhombic[39] (Ga), tetragonal (In), and rhombohedral (Bi, Sb) unit cells.

IV. RESULTS AND DISCUSSION

The two uppermost atomic layers of the most of the surface structures considered in this study [(1×3), (2×6), (4×3), and (4×4) periodicities] consist generally of the group V (more electronegative) atoms. However, in considered structures some group V atoms in the first atomic layer are replaced by the group III atoms (the atomic layers below the two uppermost layers conform to the ideal zincblende structure).

Figure 4(a) shows the present theoretical surface phase diagram for the GaSb(100) surface. It should be noted that the features of this phase diagram are in a very good agreement with the previous calculations[8] and measurements.[7] Similar surface phase diagram is shown for the InSb(100) surface in Fig. 4(b), which has not been reported earlier to our knowledge. It describes well the previous experimental findings of the (4×3) and $c(8\times2)$ reconstructions on the Sb/InSb(100).[5] It is also worth noting that the $c(8\times2)$ phase is much more stable on the InSb(100) than on the GaSb(100) one (Fig. 4). This agrees very well with experiments which show that the $c(8\times2)$ reconstruction easily forms on the InSb(100) but not on the GaSb(100) surface. To our best knowledge, there is no experimental report on the GaSb(100)$c(8\times2)$ formation. The Sb/InSb(100)$c(4\times4)$ reconstruction appears in experiments,[5] although it is not energetically stable. This can be understood due to finite temperature and configurational entropy, as we show below. The (1×3) reconstruction in Fig. 1(a) is so unstable that it is not included in Figs. 4(a) and 4(b).

The diagrams present the relative stabilities of various reconstructions (labeling is borrowed from Ref. 8). Therefore, it is interesting that the so-called surface reconstruction parameter (SRP) model explains correctly most of the rela-

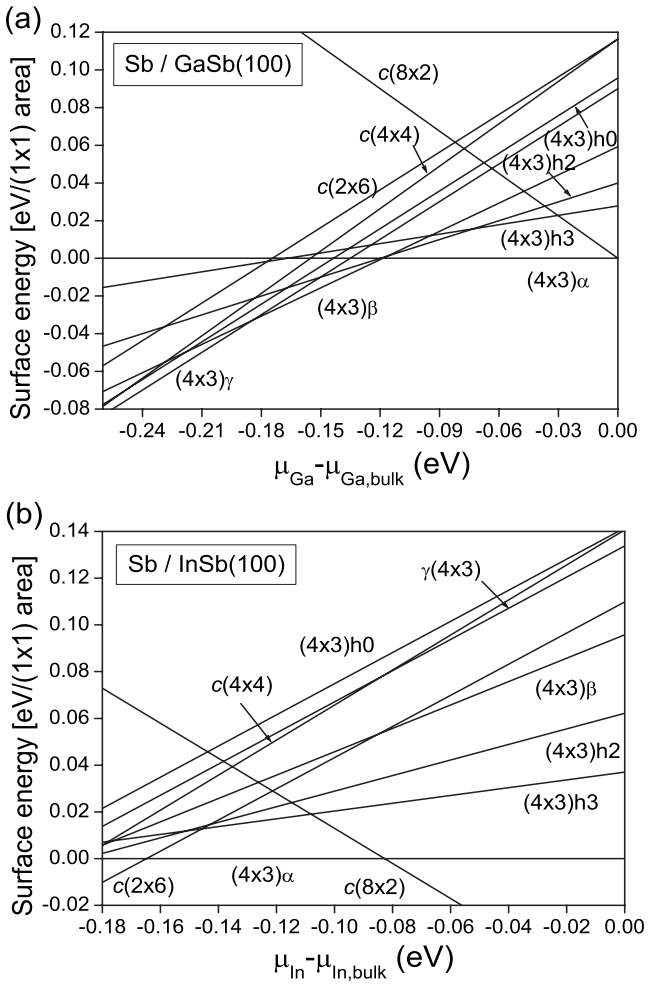

FIG. 4. Surface phase diagrams for (a) the pure Sb/GaSb(100) surface and (b) the pure Sb/InSb(100) surface. (a) The point $\mu_{Ga}=0$ eV is the Ga-rich end, and the point $\mu_{Ga}=-0.26$ eV is the Sb-rich end. (b) The point $\mu_{In}=0$ eV is the In-rich end and the point $\mu_{In}=-0.18$ eV is the Sb-rich end. The $(4\times3)\gamma$ denotes the (4×3)h0 with oblique translation vectors (Ref. 7) and the $c(8\times2)$ denotes the ζ model (Ref. 40).

tive stabilities.[41] In this model the surface stabilities are controlled by the amount of anion dangling bonds, anion homodimers, and cation homodimers. In the anion rich (AR) and cation rich (CR) conditions the SRP is obtained by following equations:

$$\mathrm{SRP_{AR}} = N_{\mathrm{a}} - N_{\mathrm{a\text{-}a}} + 2N_{\mathrm{c\text{-}c}} \tag{3}$$

$$\mathrm{SRP_{CR}} = N_{\mathrm{a}} + N_{\mathrm{a\text{-}a}}, \tag{4}$$

where N_{a} is the number of anion dangling bonds (cation dangling bonds are empty), $N_{\mathrm{a\text{-}a}}$ is the number of anion dimers, and $N_{\mathrm{c\text{-}c}}$ is the number of cation dimers. One should note that in the equations above "dimer" means any bond, in which two anion atoms or two cation atoms are connected. The relative surface energies and values for the SPR in the anion rich and cation rich conditions are shown in Table I. The anion rich and cation rich conditions correspond to the limits of the μ_{III} in the surface phase diagrams (Fig. 4). The smaller the SRP, the smaller the surface energy should be. One interesting exception from the trend predicted by the SRP is the energy difference between the (4×3)h0 and $c(2\times6)$ phases ("h0" means that there are not any heterodimers). It is interesting to compare these reconstructions, because they include only Sb-Sb dimers. The GaSb(100) surface stabilizes the (4×3)h0 compared to the $c(2\times6)$, whereas the opposite is true on the InSb(100) surface as can be noted from Fig. 4. We tested, whether this is due to the larger substrate lattice parameter of InSb by calculating relative stabilities for GaSb by using the InSb lattice parameter. These tests also showed that this is indeed the case, because the energy difference does not depend on the chosen III cation type, if the lattice parameter is kept fixed. (We note that resulting inward relaxation for the GaSb with InSb lattice parameter is similar for all reconstructions, and therefore one can compare the relative stabilities to the corresponding ones for the real GaSb and InSb surfaces.) Another reconstruction, so-called (2×3)h0m, is introduced in Fig. 2(f) to facilitate the comparison. In this reconstruction the first layer Sb-Sb dimers form the straight lines as in the $c(2\times6)$. However,

TABLE I. Surface reconstruction parameter $[1/(1\times1)$ area$]$ and relative surface energies $[\mathrm{eV}/(1\times1)$ area$]$ for the considered reconstructions on the GaSb(100) and InSb(100) surfaces in the AR and CR conditions. Note that the relative surface energies mainly follow the trends shown by the surface reconstruction parameters.

	$\mathrm{SRP_{CR}}$	$\mathrm{SRP_{AR}}$	$\mathrm{GaSb_{CR}}$	$\mathrm{GaSb_{AR}}$	$\mathrm{InSb_{CR}}$	$\mathrm{InSb_{AR}}$
$(4\times3)\alpha$	1.25	−0.25	0	0	0	0
$(4\times3)\beta$	2.25	−0.75	0.06	−0.07	0.10	0.01
$c(2\times6)$	2.67	−0.83	0.12	−0.06	0.11	−0.01
h0	2.58	−0.92	0.10	−0.08	0.14	0.02
h2	1.92	−0.58	0.04	−0.05	0.06	0.00
h3	1.67	−0.33	0.03	−0.02	0.04	0.01
$c(4\times4)$	1.88	−0.63	0.12	−0.08	0.14	0.01
h0m	2.67	−1.00	0.12	−0.06	0.11	−0.01

TABLE II. Relative surface energies [eV/(1×1) area] for the (4×3)h0 and (2×3)h0m reconstructions. First row corresponds to the fully relaxed case. In the second row only the dimers are allowed to relax parallel to surface. Next, the rest of the first- and second-layer atoms are allowed additionally relax either in the $[0\bar{1}1]$ direction or in the [011] direction. In the last case all the first- and second-layer atoms are allowed to fully relax. Note that the relative contributions of the relaxations in the $[0\bar{1}1]$ and [011] directions to the total energy of the (4×3)h0 reconstruction depend on the substrate.

	GaSb-h0	GaSb-h0m	InSb-h0	InSb-h0m
Fully relaxed	0.000	0.021	0.000	−0.031
Dimers	0.164	0.144	0.136	0.122
Dimers+$[0\bar{1}1]$	0.113	0.144	0.121	0.122
Dimers+[011]	0.138	0.113	0.102	0.064
First and second layers	0.087	0.113	0.087	0.064

the second-layer Sb-Sb dimers do not allow centered unit cell in difference to the $c(2\times6)$. This (2×3)h0m reconstruction is also metallic ("m" stands for metallic), and therefore it should not be stable according to the ECM. Total energy for the (2×3)h0m is almost the same as for the $c(2\times6)$ of the Sb/GaSb and Sb/InSb [~1 meV/(1×1) area less stable].

It is noted that the average first-layer Sb-Sb dimer bond length is shorther in the (2×3)h0m reconstruction (2.85 Å on GaSb and 2.87 Å on InSb) than in the (4×3)h0 reconstruction (2.90 Å on GaSb and InSb). This is probably due to the mutual interaction of dimers in the dimer rows in the (2×3)h0m reconstruction. If one of the dimers is removed, the average dimer bond length is increased to 2.93 Å. Even if the new dangling bonds were passivated, the dimer bond lengths are larger (2.90 Å) than in the original (2×3)h0m reconstruction. This relatively strong interaction in the dimer rows probably stabilizes the (2×3)h0m and (2×6) reconstructions. However, the violation of the ECM destabilizes these surfaces. We performed constrained calculations to analyze the situation further. All atoms were allowed to relax from the ideal (bulk) positions in the [100] direction (except the fixed ones at the bottom surface). However, the positions in the $[0\bar{1}1]$ and [011] directions were constrained. In the first step only the first- and second-layer Sb dimer atoms were allowed to relax. Then the rest of the first- and second-layer atoms were allowed to relax only in the $[0\bar{1}1]$ direction or [011] direction. Finally, all the first- and second-layer atoms were allowed to fully relax. Results are shown in Table II. First, one can note that the relative-energy differences of the considered structures obtained by allowing full relaxation only in the two topmost atomic layers agree well with the corresponding ones obtained by the fully relaxed systems. The energy of the (2×3)h0m reconstruction is not decreased by allowing relaxation in the $[0\bar{1}1]$ direction, which is due to the nonexistence of the holes in the dimer rows. On the other hand, the relaxation in the $[0\bar{1}1]$ direction decreases significantly the energy of the (4×3)h0 reconstruction. However, the relaxation in the [011] direction becomes more important

TABLE III. Displacements (Å) of the second-layer Sb atoms (see Fig. 2) from the ideal (bulk) positions in the [011] direction for the (4×3)h0 and (2×3)h0m reconstructions.

	GaSb-h0	GaSb-h0m	InSb-h0	InSb-h0m
Sb0	0.000	0.026	0.064	0.142
Sb1	−0.001	0.026	0.064	0.142
Sb2	0.070	0.100	0.069	0.143
Sb3	0.002	0.100	0.068	0.143

for the (4×3)h0 as well, when the substrate is changed from GaSb to InSb. The atomic shifts from the ideal positions in the [011] direction for the second-layer Sb atoms [see Fig. 2(a)] in the dimer rows are shown in Table III. It is realized that these shifts are much larger on the InSb surface. However, the shifts are strongly decreased for some atoms in the (4×3)h0 reconstruction due to the dimer, which is displaced from the dimer row. We conclude that when the substrate lattice parameter is increased, it becomes energetically more favorable for the surface to shrink in the dimer rows. However, the displaced dimer in the (4×3)h0 reconstruction restricts this relaxation destabilizing the surface. This phenomenon is basically the same for all semiconducting (4×3) reconstructions thus explaining the increased stability of the metallic $c(2\times6)$ and (2×3)h0m reconstructions.

The energy differences are, however, quite small in the anion rich conditions on the Sb/InSb surfaces as one can note from Fig. 4(b). The situation is different for the Bi/InSb surface as shown in Figs. 5(a) and 5(b). The end numbering of the model with "2" means that Bi atoms occupy the group-V sites in the two topmost layers (otherwise, there is only one layer of Bi). One should note that for clarity and comparison with Fig. 4, the total energies for the reconstructions with two Bi layers on top are not shown in Fig. 5(a). However, they are quite unstable and do not change the relative stabilities close to the ground state in Sb-rich conditions. In In-rich conditions their role gets rapidly smaller as the chemical potential of Bi is decreased [around $\mu_{\mathrm{Bi}}-\mu_{\mathrm{Bi,bulk}}=-0.05$ eV only total energy for the $(4\times3)\alpha$-2 is significantly lower than that of the $(4\times3)\alpha$].

One should note that the Bi-induced $c(2\times6)$ reconstruction has a large stability area and the energy differences are larger for the Bi/InSb surface [The (2×3)h0m reconstruction (not shown) is slightly less stable, about 5 meV per (1×1) surface area]. However, the energy differences are still rather small. Therefore, we recalculated the surface phase diagram for the Bi/InSb surface by using the generalized gradient approximation (GGA). The resulting phase diagram is quite similar to that obtained by the LDA [$(4\times3)\alpha$ and (4×3)h3 structures are destabilized more notably, but qualitatively all features are the same]. Especially, the $c(2\times6)$ reconstruction is found to be the ground state also within the GGA (Ref. 42) (a=4.70 Å). Because the energy differences are small between various reconstructions, we also estimate the effect of finite temperature by including configurational entropy according to the model in the Ref. 43 in the Sb- and Bi-rich conditions. The statistical probability c_i of a particular reconstruction i is obtained as:

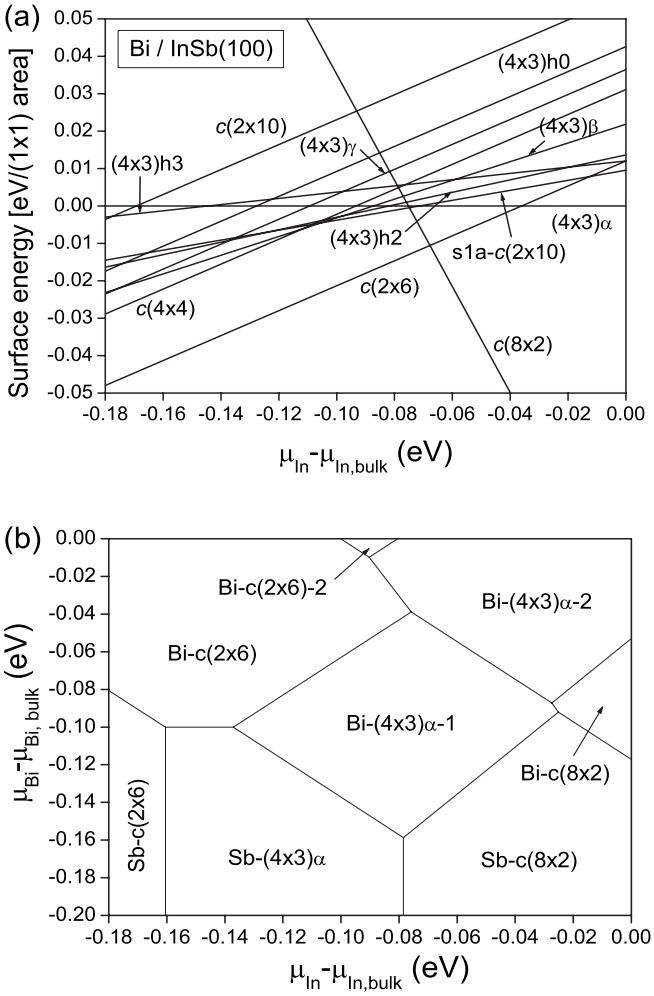

FIG. 5. Surface phase diagrams for the Bi/InSb(100) surface: (a) $\mu_{Bi}=\mu_{Bi,bulk}$; one should note that for clarity and comparison with Fig. 4, the reconstructions with two Bi layers on top are not shown. (b) μ_{Bi} is variable. The point $\mu_{Bi}=0$ eV is the Bi-rich end, the point $\mu_{In}=0$ eV is the In-rich end, and the point $\mu_{In}=-0.18$ eV is the Sb-rich end. The $(4\times3)\gamma$ denotes the (4×3)h0 with oblique translation vectors (Ref. 7) and the $c(2\times10)$ and s1a-$c(2\times10)$ reconstructions are from the Ref. 23. The configuration of the (4×3)h3 was chosen to allow comparison with Ref. 8. If the homodimer was in the middle of the heterodimers, the total energy would be decreased by 5 meV per (1×1) area. The total energy of the (4×3)h2 is practically unchanged, if the one heterodimer on the right side is shifted to the middle of the homodimers.

$$Z_i = g_i \exp[-\gamma_i^0(\mu_{\mathrm{In}},\mu_{\mathrm{Bi}})A/k_BT], \tag{5}$$

$$Z = \sum_{i\in S} Z_i, \tag{6}$$

$$c_i = \frac{z_i}{z}, \tag{7}$$

where the Z is the partition function, which is defined independently for each unit cell of area A, γ_i^0 is the surface energy at 0 K, and g_i is a symmetry-determined degeneracy factor. The set of structures S includes all structures represented in Fig. 5(a) and additionally all such structures, in which the first layer dimer shifted from the dimer row (i.e., the dimer in the upper left corner in Fig. 2) does not include a group III (Ga, In) atom. We also calculated structures, in which the atoms in heterodimers are interchanged, but these structures are very unstable, and therefore they contribute to the partition function Z only marginally. The statistical probability for the metallic phases $c(2\times6)$ and (2×3)h0m are about 0.17 (17%) and 0.14 (14%) at 300 K (around the measuring temperature), respectively, and about 0.11 (11%) and 0.10 (10%) at 500 K (around the heating temperature). The probability of the $c(2\times6)$ is largest at 300 K, whereas the probability of the (4×3)h2 reconstruction is largest at 500 K. The energy associated in the phase boundaries can change these results to a some extent. However, our tests [performed by (8×3) cells] showed that these energies are only of the order of some millielectron volts per (1×1) area. These results are in accordance with the results of Ref. 44, in which it was shown that the energies associated with phase boundaries due to disorder are small for the GaSb(100)(4×3) reconstructions. The probability of the metallic phases is probably larger within the GGA due to the destabilization of several phases. However, the probability of the semiconducting phases is still remarkable. Although the above values are not considered as quantitative results, it is concluded that it is probable to find different phases in measurements. As noted in the introduction, the disorder of the (4×3) building blocks leads to the $c(2\times6)$ diffraction pattern for the GaSb.[24] We suppose that this is true also for the Bi/InSb and that the unordered pattern of the $c(2\times6)$ and (2×3)h0m can also lead to the $c(2\times6)$ diffraction pattern. The probability of the $c(4\times4)$ is only 7–8 % depending on the considered temperature (300–500 K).

We recall that the exceptional stability of the (2×1) reconstruction on the Bi/GaAs(100) and Bi/InP(100) surfaces was recently connected to the pseudogap formation and surface-stress relief. These effects were connected to the particular surface geometry due to the Bi atom size (e.g., the angle between the backbonds is rather small for the Bi-stabilized surfaces).[21,22] Although the metallicity induces states in the energy gap, relative stability compared to other reconstructions is achieved by pushing a rather dispersionless occupied state dominantly of the Bi character deeper from the Fermi level in the direction of dimer rows in k space. Electronic charge-density contours show increased interaction in the dimer rows.[22] For the Bi-stabilized and Sb-stabilized $c(2\times6)$ reconstructions it is hard to find significant differences in the density of states. However, the dimer length is larger and the backbond angles are smaller for the Bi-stabilized surfaces than for the Sb-stabilized surfaces as in the case of the V/GaAs(100)(2×1) surfaces (V=As, Sb, Bi). Therefore, it is probable that the bonding configuration increases also the stabilization of the more complex metallic $c(2\times6)$ and (2×3)h0m reconstructions on the Bi/InSb(100) surface, because these reconstructions include also dimer rows. Below, it is shown that the coexistence of the energetically stable structures explain the measurements of the Bi/InSb(100)$c(2\times6)$ surface.

The measured I-V curves in Fig. 6(a) show that both metallic and semiconducting areas appear on the

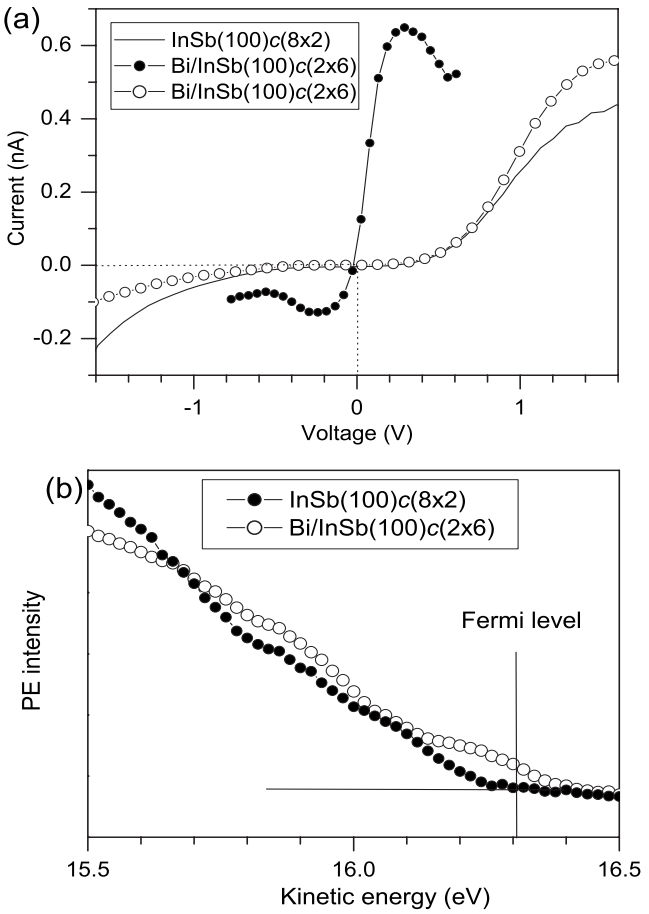

FIG. 6. (a) Current-voltage curves measured by STS mode from the InSb(100)$c(8\times2)$ area and two different areas on the Bi/InSb(100)$c(2\times6)$ surface; the dotted lines represent zero levels. (b) Valence-band photoemissions near the Fermi level (vertical line) measured from the InSb(100)$c(8\times2)$ and Bi/InSb(100)$c(2\times6)$ surfaces. The Fermi energy was determined from a Ta plate connected to the sample holder. The horizontal line is a zero-emission level.

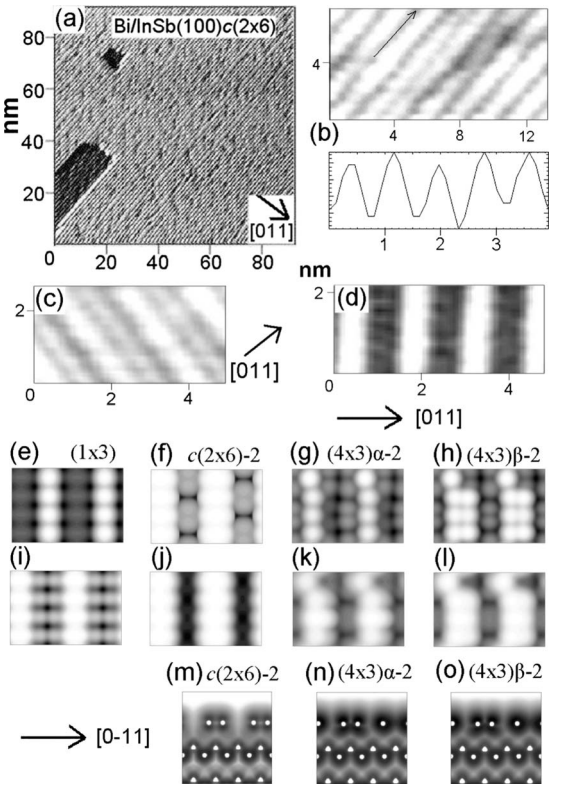

FIG. 7. (a) Large-scale filled-state STM image measured from the Bi/InSb(100)$c(2\times6)$ surface; $I=0.16$ nA and $V=1.67$ V. (b) Measured filled-state image with the line profile along the black arrow; $I=0.19$ nA and $V=0.95$ V. (c) Measured filled-state image; $I=0.05$ nA and $V=1.04$ V. (d) Measured empty-state image; $I=0.07$ nA and $V=1.00$ V. (e)–(h) Calculated filled-state STM images (1.00 V) for the (1×3), $c(2\times6)$-2, $(4\times3)\alpha$-2, and $(4\times3)\beta$-2 structures. (i)–(l) Calculated empty-state STM images (1.00 V) for the (1×3), $c(2\times6)$-2, $(4\times3)\alpha$-2, and $(4\times3)\beta$-2 structures. (m)–(o) Calculated filled-state contours between the white rows for the $c(2\times6)$-2, $(4\times3)\alpha$-2, and $(4\times3)\beta$-2 structures.

Bi/InSb(100)$c(2\times6)$ surface. The presented I-V curves are average curves of grid-point measurements over well-ordered areas of the topographic image, which was measured at the same time as the I-V curves. It is worth noting that different set-point voltages and STM tips produced the same results as shown in Fig. 6. Thus, these STS results showing the presence of metallic Bi/InSb(100)$c(2\times6)$ areas give a strong evidence for the violation of the ECM, since a metallic III-V reconstruction never obeys the ECM. The occurrence of both the metallic and semiconducting areas can be understood with the formation of areas with the $c(2\times6)$ or (2×3)h0m structure and areas with the (4×3) structures. The valence-band spectra near the Fermi level in Fig. 6(b) support the existence of metallic areas on the Bi/InSb(100)$c(2\times6)$ surface because it produces a small photoemission signal from the Fermi level, as compared to the semiconducting InSb(100)$c(8\times2)$ substrate. In passing, Bi might be a useful surfactant for the epitaxial growth of III-Sb materials since the metallic Bi-stabilized $c(2\times6)$ growth front of III-Sb substrates can be expected to lead to an increase in the III-atom diffusion on the growing surface and, therefore, to improved III-Sb layers.[45]

Figure 7 presents measured STM images of the Bi/InSb(100)$c(2\times6)$ surface as well as the calculated images for the (1×3), $c(2\times6)$-2, $(4\times3)\alpha$-2, and $(4\times3)\beta$-2 structures. The $(4\times3)\alpha$ and $(4\times3)\beta$ phases represent different possible (4×3) configurations. The calculated images for the structures, where Bi atoms occupy only the topmost sites and Sb atoms occupy the second-layer sites, are very similar to those shown in Fig. 7. The measured filled-state STM images are presented in Figs. 7(a)–7(c) and empty-state image in Fig. 7(d) while the calculated filled-state and empty-state images are shown, respectively, in Figs. 7(e)–7(l). The comparison of the measured and calculated STM results reveals that the measured surface includes areas, which agree better with the $c(2\times6)$ model than with the other ones, due to the following reasons. First, the $c(2\times6)$ model is more suitable than the (1×3) one since in dual-polarity measurements (not shown), the white rows were found to be aligned in the filled- and empty-state images and since two gray protrusion lines of the simulated (1×3) empty-state image are not seen between the white rows in Fig. 7(d). Second, the

$c(2\times6)$ structure agrees better with Figs. 7(b)–7(d) than the $(4\times3)\alpha$ model since in the filled-state measurements, only a single centered line of gray features is seen between the white rows and since the clear $4\times$ kinks of the $(4\times3)\alpha$ phase in the empty-state image are not seen in the measured image of Fig. 7(d). Third, the calculated $c(2\times6)$ images agree with the measurements better than the $(4\times3)\beta$ images since the apparent $4\times$ kinks of the simulated $(4\times3)\beta$ images in the both filled and empty states are not seen in Figs. 7(c) and 7(d). It should be noted that the width of the white rows appears to depend on the measurement current, as seen in Figs. 7(b) and 7(c), and therefore it cannot be used as a proper criterion. Finally, the line profile below the image of Fig. 7(b), which is taken along the black arrow between the white rows in the measured image, further supports the presence of the $c(2\times6)$ areas since the profile shows the $2\times$ periodicity that is inconsistent with the (1×3) and (4×3) phases, as can be deduced from the simulated contours in Figs. 7(m)–7(o). The distance between the peaks in Fig. 7(b) is about 0.8 nm, which is much closer to the theoretical value for the $c(2\times6)$ structure (0.9 nm) than to that of the $(4\times3)\alpha$ and $(4\times3)\beta$ structures (0.45 nm). Due to the limited measurement resolution, individual peaks of the dimer atoms cannot be seen in the measured line profile. Our STM observations [e.g., Figs. 7(a) and 7(b)] clearly show that the measured surfaces are not uniform, and cannot be described only with the $c(2\times6)$ phase [i.e., the presence of the other phases is not excluded], in agreement with the above STS findings and the SCLS results below. It is also worth noting that the $c(2\times6)$ LEED found above does not exclude the presence of (4×3) areas too since the recent findings show that the (1×3) and $c(2\times6)$ patterns can arise from different types of disorder of the (4×3) units.[24]

The measured Bi $5d$, Sb $4d$, and In $4d$ spectra of the Bi/InSb(100)$c(2\times6)$ surface were fitted by means of the minimum number of the components. Thus, in the comparison of measured and calculated SCLSs below, an important criterion is that the calculated maximum and minimum SCLSs agree reasonably with the measured SCLSs since the smaller shifts are most likely unresolved in the experiments. On the other hand, the absence of the smaller SCLSs in the measurements of course does not exclude the presence of the phases producing only the smaller shifts. In the case of the Bi $5d$ shifts, the separation between different components is a reasonable criterion since the 0 eV references for the measured and calculated Bi shifts are not aligned. The resulted fittings show that both the Sb $4d$ and In $4d$ spectra in Fig. 8 include at least two SCLSs, and the Bi $5d_{5/2}$ emission in Fig. 9 includes at least three different components. The Gaussian widths of the Bi peaks were larger than those of the Sb and In peaks, reflecting an expected increase in inhomogeneity in the bonding environment of the Bi adsorbate atoms, as compared to the Sb and In bonding environments. The previous Sb $4d$ SCLS studies for the Sb/GaSb(100)$c(2\times6)$ surface have revealed two different bonding sites for the group-V atoms in this surface structure.[1,2] We propose that a third Sb SCLS was not resolved previously due to the presence of the bulk emission, which usually hinders resolving SCLSs. Taking into account possible errors in the former and present fitting procedures, the separation of the two Sb SCLSs (about 0.87 eV)[2] is in a reasonable agreement with the separation (0.63 eV) between the Bi components S3 and S1 in Fig. 9. Therefore, it appears that the S2-like component was not resolved previously on the Sb/GaSb(100)$c(2\times6)$.

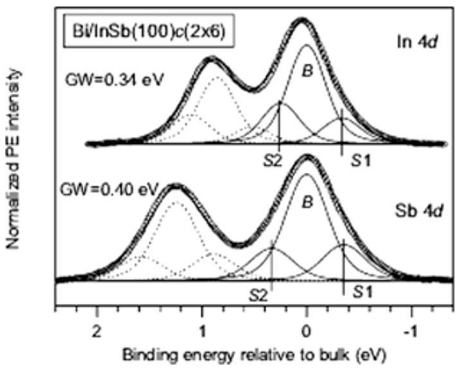

FIG. 8. Fitted Sb and In $4d$ core-level spectra of the Bi/InSb(100)$c(2\times6)$ surface. The fitting parameters are: spin-orbit split is 1.243 (0.855) eV, branching ratio is 0.65–0.73 (0.65–0.73), Lorentzian width is 0.16 (0.16) eV, and Gaussian width is 0.40 (0.35) eV for the Sb (In) spectrum. The $d_{5/2}$ peaks of the bulk (B) and surface (S) components are shown by solid lines. The photon energy and electron-emission angle are 70 eV and 0° for Sb and 50 eV and 0° for In.

The comparison between the calculated and measured SCLSs in Table IV shows that none of the models alone describes the all measured SCLSs well, which supports the coexistence of two or more phases on the Bi/InSb(100)$c(2\times6)$ surface measured. The two-phase combinations of $c(2\times6)$ and $c(2\times6)$-2 as well as of $(4\times3)\alpha$ and $(4\times3)\alpha$-2 do not improve much the agreement between the calculated and measured SCLSs. Note that in the combination of $(4\times3)\alpha$ and $(4\times3)\alpha$-2, the separation of the calculated Bi shifts increases to 0.99 eV. In contrast, the SCLSs of the $c(2\times6)$ and $(4\times3)\alpha$ phases complete each other better and together they improve the agreement with the measurements and calculations. The comparison of the calculated and measured SCLSs also indicates that the Bi atoms appear in both the first (topmost) and second layers. Furthermore, the atomic origins of the Bi shifts S1, S2, and S3 are studied by means of the calculations. In the $c(2\times6)$-2 structure, the calculated Bi

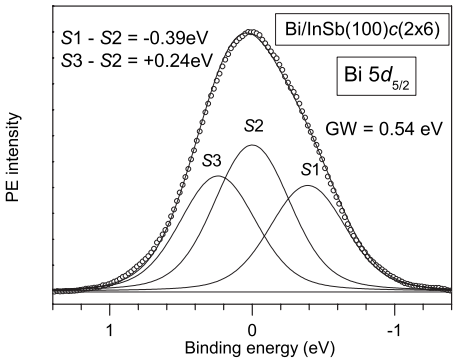

FIG. 9. Fitted Bi $5d_{5/2}$ core-level peak from the Bi/InSb(100)$c(2\times6)$ surface with the photon energy of 70 eV and 60° emission. The Lorentzian width is 0.16 eV and the Gaussian width is 0.54 eV.

TABLE IV. Measured surface core-level shifts (eV) and calculated ones (by VASP *ab initio* code) for the energetically stable structures of the Bi/InSb(100) surface within the initial-state model. Negative value indicates smaller binding energy (BE) as compared to the 0 eV reference, which is the bulk BE for the In 4*d* and Sb 4*d* levels. For the calculated Bi 5*d* shifts, the topmost dimer in the 4× kink site of the $(4\times3)\alpha$ phase is taken as the 0 eV reference. In contrast, the measured Bi spectrum has been aligned by setting *S*2 at 0 eV. Because the 0 eV references for the measured and calculated Bi shifts are not aligned, the energy separation of different Bi shifts rather than individual shifts should be compared. Calculated shifts smaller than 0.05 eV are not listed.

	Calculated $c(2\times6)$	Calculated $c(2\times6)-2$	Calculated $(4\times3)\alpha$	Calculated $(4\times3)\alpha$-2	Measured
In 4*d*	+0.10	−0.09	−0.21, +0.23, +0.48	−0.26, −0.10, +0.14, +0.35	−0.33, +0.25
Sb 4*d*	+0.18, +0.35	+0.19	−0.37, −0.22, −0.12, +0.10, +0.38, +0.51	−0.12	−0.35, +0.33
Bi 5*d*	+0.23	−0.29, −0.06, +0.11	0, +0.17, +0.34	−0.65, −0.53, −0.37, −0.31, −0.18, −0.11, +0.10	−0.39, 0, +0.24

shifts −0.29, −0.06, and +0.11 eV arise, respectively, from the dimers in the second layer, from the second-layer Bi atoms below the topmost dimers, and from the topmost dimer. In the $(4\times3)\alpha$ structure, the shifts 0, +0.17, and +0.34 eV are caused by the topmost dimers in the 4× kink site, in the site next to the kink, and in the middle of the three-dimer stack, respectively. For the $(4\times3)\alpha$-2 structure, the origins of three highest BE shifts are similar to those of the $(4\times3)\alpha$, and the lower BE shifts −0.31, −0.37, −0.53, and −0.65 eV all arise from the second-layer atoms, respectively, in the sites below the middle dimers, in the dimer sites, in the corner sites of the dimer stack, and in the sites below the kink dimer. Combining these origins, we propose that the highest BE shift S3 arises from the topmost Bi dimers (excluding the 4× kink dimers), the middle shift S2 is caused by the kink dimers and a part of the second-layer Bi atoms below the topmost dimers, and that the lowest BE shift S1 is caused by the second-layer dimers and the other second-layer Bi atoms below the dimers.

V. CONCLUSIONS

The first-principles phase diagrams clearly demonstrate that the metallic $c(2\times6)$ structure is stabilized in relation to the other phases, when the substrate lattice constant is increased (GaSb→InSb). This stabilization is attributed to the partial prohibition of the relaxation in the direction perpendicular to dimer rows in the competing reconstructions. The addition of Bi to the surface stabilizes further the metallic $c(2\times6)$ reconstruction, which is due to the particular stability of the Bi dimer rows. In addition to our former results of the (2×1) reconstruction on the Bi/GaAs(100) and Bi/InP(100) surfaces,[21,22] the present finding is a further example of the Bi-stabilized surface reconstruction, which does not obey the ECM. The former result was for the Ga-(or In-) rich conditions, whereas the present result is particularly for the Sb-rich conditions. Our findings are in accordance with those of Chuasiripattana and Srivastava,[12] who attributed the metastability of the $c(2\times6)$ reconstruction on the GaSb(100) surface to the significant elastic deformation in the top atomic layers of the surface. It is somewhat surprising that the ECM is not obeyed on the Bi-stabilized surface. On the other hand, one has to remember that the induced density of states at Fermi level is very low, and therefore it can be compensated.

These theoretical results explain our experimental findings well. First of all, the energetic stability of the metallic $c(2\times6)$ phase agrees with the STS and photoemission measurements that give a strong evidence for the existence of metallic reconstruction on the Bi/InSb(100)$c(2\times6)$ sample. The comparison of the calculated and measured STM results supports the occurrence of areas with the $c(2\times6)$ atomic structure. The STM and STS measurements show that the atomic structure of the Bi/InSb(100)$c(2\times6)$ sample is not uniform and that the measured surface also includes semiconducting areas, which can be understood by the coexistence of areas with the stable metallic $c(2\times6)$ structure and areas with the stable semiconducting (4×3) structure. This is supported by the first-principles phase diagram and by the comparison of the calculated and measured photoelectron BE shifts. The atomic origins have been proposed for the Bi 5*d* SCLSs of the Bi/InSb(100)$c(2\times6)$ surface.

ACKNOWLEDGMENTS

We are grateful to H. Ollila and to the MAX laboratory staff for their assistance. The financial support by the Transnational Access to the Research Infrastructure Program (TARI) is acknowledged. This work has been supported by the Academy of Finland under Grants No. 122743 (P.L.) and No. 122355 (I.J.V.) as well as Finnish Academy of Sciences and Letters (P.L.). The calculations were performed using the facilities of the Finnish Centre for Scientific Computing (CSC) and the Mgrid project (Turku, Finland). The Swedish Research Council (L.V and B.J.), the Swedish Foundation for Strategic Research (L.V. and B.J.), the Hungarian Scientific Research Fund (Grant No. T048827) (L.V.), the Carl Tryggers Foundation (M.P.J.P.), the Turku University Foundation (M.P.J.P.), and the Emil Aaltonen Foundation (M.P.J.P.) are also acknowledged for financial support.

*pekka.laukkanen@utu.fi
†marko.punkkinen@utu.fi

[1] G. E. Franklin, D. H. Rich, A. Samsavar, E. S. Hirschorn, F. M. Leibsle, T. Miller, and T.-C. Chiang, Phys. Rev. B **41**, 12619 (1990).
[2] M. T. Sieger, T. Miller, and T.-C. Chiang, Phys. Rev. B **52**, 8256 (1995).
[3] A. G. de Oliveira, S. D. Parker, R. Droopad, and B. A. Joyce, Surf. Sci. **227**, 150 (1990).
[4] J. Olde, K.-M. Behrens, H.-P. Barnscheidt, R. Manzke, M. Skibowski, J. Henk, and W. Schattke, Phys. Rev. B **44**, 6312 (1991).
[5] C. F. McConville, T. S. Jones, F. M. Leibsle, S. M. Driver, T. C. Q. Noakes, M. O. Schweitzer, and N. V. Richardson, Phys. Rev. B **50**, 14965 (1994).
[6] U. Resch-Esser, N. Esser, B. Brar, and H. Kroemer, Phys. Rev. B **55**, 15401 (1997).
[7] W. Barvosa-Carter, A. S. Bracker, J. C. Culbertson, B. Z. Nosho, B. V. Shanabrook, L. J. Whitman, Hanchul Kim, N. A. Modine, and E. Kaxiras, Phys. Rev. Lett. **84**, 4649 (2000).
[8] M. C. Righi, R. Magri, and C. M. Bertoni, Phys. Rev. B **71**, 075323 (2005).
[9] C. B. Duke, Chem. Rev. (Washington, D.C.) **96**, 1237 (1996).
[10] D. J. Chadi, J. Vac. Sci. Technol. A **5**, 834 (1987).
[11] M. D. Pashley, Phys. Rev. B **40**, 10481 (1989).
[12] K. Chuasiripattana and G. P. Srivastava, Surf. Sci. **600**, 3803 (2006).
[13] J. K. Shurtleff, R. T. Lee, C. M. Fetzer, and G. B. Stringfellow, Appl. Phys. Lett. **75**, 1914 (1999).
[14] C. M. Fetzer, R. T. Lee, J. K. Shurtleff, G. B. Stringfellow, S. M. Lee, and T. Y. Seong, Appl. Phys. Lett. **76**, 1440 (2000).
[15] Ph. Hofmann, Prog. Surf. Sci. **81**, 191 (2006).
[16] S. Cho, Y.-H. Um, Y. Kim, G. K. L. Wong, J. B. Ketterson, and J. Hong, J. Vac. Sci. Technol. A **20**, 1191 (2002).
[17] Y.-Q. Xu, B.-G. Liu, and D. G. Pettifor, Phys. Rev. B **66**, 184435 (2002).
[18] L. J. Whitman, P. M. Thibado, S. C. Erwin, B. R. Bennett, and B. V. Shanabrook, Phys. Rev. Lett. **79**, 693 (1997).
[19] P. Moriarty, P. H. Beton, M. Henini, and D. A. Woolf, Surf. Sci. **365**, L663 (1996).
[20] P. Laukkanen, J. Pakarinen, M. Ahola-Tuomi, M. Kuzmin, R. E. Perälä, I. J. Väyrynen, A. Tukiainen, J. Konttinen, P. Tuomisto, and M. Pessa, Phys. Rev. B **74**, 155302 (2006).
[21] P. Laukkanen, M. P. J. Punkkinen, H.-P. Komsa, M. Ahola-Tuomi, K. Kokko, M. Kuzmin, J. Adell, J. Sadowski, R. E. Perälä, M. Ropo, T. T. Rantala, I. J. Väyrynen, M. Pessa, L. Vitos, J. Kollár, S. Mirbt, and B. Johansson, Phys. Rev. Lett. **100**, 086101 (2008).
[22] M. P. J. Punkkinen, P. Laukkanen, H.-P. Komsa, M. Ahola-Tuomi, N. Räsänen, K. Kokko, M. Kuzmin, J. Adell, J. Sadowski, R. E. Perälä, M. Ropo, T. T. Rantala, I. J. Väyrynen, M. Pessa, L. Vitos, J. Kollár, S. Mirbt, and B. Johansson, Phys. Rev. B **78**, 195304 (2008).
[23] J. Houze, S. Kim, S.-G. Kim, S. C. Erwin, and L. J. Whitman, Phys. Rev. B **76**, 205303 (2007).
[24] O. Romanyuk, V. M. Kaganer, R. Shayduk, B. P. Tinkham, and W. Braun, Phys. Rev. B **77**, 235322 (2008).
[25] Y. Chao, K. Svensson, D. Radosavkic, V. R. Dhanak, M. R. C. Hunt, and L. Siller, Phys. Rev. B **66**, 075323 (2002).
[26] D. M. Ceperley and B. J. Alder, Phys. Rev. Lett. **45**, 566 (1980).
[27] J. P. Perdew and A. Zunger, Phys. Rev. B **23**, 5048 (1981).
[28] P. E. Blöchl, Phys. Rev. B **50**, 17953 (1994).
[29] G. Kresse and D. Joubert, Phys. Rev. B **59**, 1758 (1999).
[30] G. Kresse and J. Hafner, Phys. Rev. B **47**, 558 (1993).
[31] G. Kresse and J. Hafner, Phys. Rev. B **49**, 14251 (1994).
[32] G. Kresse and J. Furthmüller, Comput. Mater. Sci. **6**, 15 (1996).
[33] G. Kresse and J. Furthmüller, Phys. Rev. B **54**, 11169 (1996).
[34] H. J. Monkhorst and J. D. Pack, Phys. Rev. B **13**, 5188 (1976).
[35] M. P. J. Punkkinen, P. Laukkanen, K. Kokko, M. Ropo, M. Ahola-Tuomi, I. J. Väyrynen, H.-P. Komsa, T. T. Rantala, M. Pessa, M. Kuzmin, L. Vitos, J. Kollár, and B. Johansson, Phys. Rev. B **76**, 115334 (2007).
[36] M. P. J. Punkkinen, K. Kokko, L. Vitos, P. Laukkanen, E. Airiskallio, M. Ropo, M. Ahola-Tuomi, M. Kuzmin, I. J. Väyrynen, and B. Johansson, Phys. Rev. B **77**, 245302 (2008).
[37] N. Moll, A. Kley, E. Pehlke, and M. Scheffler, Phys. Rev. B **54**, 8844 (1996).
[38] W. G. Schmidt and F. Bechstedt, Phys. Rev. B **55**, 13051 (1997).
[39] M. Bernasconi, G. L. Chiarotti, and E. Tosatti, Phys. Rev. B **52**, 9988 (1995).
[40] S.-H. Lee, W. Moritz, and M. Scheffler, Phys. Rev. Lett. **85**, 3890 (2000).
[41] S. Mirbt, N. Moll, A. Kley, and J. D. Joannopoulos, Surf. Sci. **422**, L177 (1999).
[42] J. P. Perdew, K. Burke, and M. Ernzerhof, Phys. Rev. Lett. **77**, 3865 (1996).
[43] E. Penev, P. Kratzer, and M. Scheffler, Phys. Rev. Lett. **93**, 146102 (2004).
[44] O. Romanyuk, F. Grosse, and W. Braun, Phys. Rev. B **79**, 235330 (2009).
[45] J. Neugebauer, T. K. Zywietz, M. Scheffler, J. E. Northrup, H. Chen, and R. M. Feenstra, Phys. Rev. Lett. **90**, 056101 (2003).